From Plasma Jets to Pulsed Laser: A Comparative Spectroscopic Perspective on Copper Emission

1st Muna A. Issa*
Department of Physics, College of Education,
Mustansiriyah University,
Baghdad, Iraq
dr.munaahmed@uomustansiriyah.edu.iq

2nd Ahmed S. Jaber
Information and Communication Technology Research Center,
Scientific Research Commission,
Baghdad, Iraq
sawsanhussein1976@gmail.com

3rd Sawsan H. Abdullah
Information and Communication Technology Research Center,
Scientific Research Commission,
Baghdad, Iraq
ahmedcctv11@gmail.com

*Corresponding author: dr.munaahmed@uomustansiriyah.edu.iq
Received: 2026-07-06; **Accepted:** 2026-08-10

***Abstract*—Two approaches were applied to the spectroscopic study of plasma: the plasma jet technique and the pulsed laser. The plasma from the Neodymium-doped Yttrium Aluminum Garnet (Nd:YAG) laser had much higher Cu I emission than the plasma jet, which could be related to the better excitation and ablation of the plasma. The plasma jet produced a wider range of spectra with strong contributions of Ar I and N2/N2+. This indicates an excitation that is continuous and driven by gases. As for electron temperatures, the plasma created by the laser showed high temperatures, ranging from 0.869 to 0.884 eV, very different from the plasma jet readings, in the range of 0.501 to 0.621 eV. This indicates that laser ablation is more effective in heating electrons due to its fast and localized nature. The plasma jet density rose from 1.216 x 10^18 cm^-3 to 1.351 x 10^18 cm^-3 as the argon flow rate increased, and the laser plasma density rose from 1.146 x 10^18 cm^-3 to 1.251 x 10^18 cm^-3 as the pulse energy increased. Even with the laser plasma showing a higher electron temperature, the plasma jet reached a higher peak electron density for the specific conditions of the experiment. The plasma jet had a Debye length between 4.77 x 10^-6 and 5.04 x 10^-6 cm, and its Debye numbers were between 553 and 723. This suggests more robust electrostatic shielding and a smaller plasma. On the other hand, the Nd:YAG laser plasma had larger Debye lengths from 6.25 x 10^-6 to 6.47 x 10^-6 cm, and its Debye numbers were significantly larger, ranging from 1277 to 1299.**

Keywords—spectroscopic, plasma parameters, plasma jet, pulsed laser deposition, copper, SPSS.

I. Introduction

Plasma, fundamentally an ionized gas, consists of molecules, ions, and electrons [1]. On a larger scale, positive ions and negative electrons tend to be in balance. Atoms can become ionized into positive ions and electrons when they absorb sufficient environmental energy to overcome their thermal and binding energies; subsequently, these particles interact electromagnetically [2]. Plasma deposition of copper nanoparticles has great significance in materials science. This is due to their unique properties and numerous potential applications [3]. Copper plasma, mainly produced by pulsed laser deposition (PLD) or atmospheric plasma jet (APJ), is commonly used to deposit thin layers of copper-based compounds such as CuO [4]. These films are then indispensable to many applications such as gas sensors [5], transparent conductors [6], and even photocatalysts [7]. PLD has excellent control over the composition, thickness, and microstructure of films produced from solid targets with respect to the laser settings and the plasma characteristics [8].

Atmospheric plasma jets are also used to coat copper-based materials for surface properties such as being more resistant to rust, antibacterial, and improved electrical performance [9]. Copper and its oxides (CuO and Cu_2O) are very attractive because of their many benefits, and they are cheap [10]. Standard atmospheric plasma jets produce non-equilibrium plasma, wherein electrons gain significant energy from the electric field while heavier particles remain at much lower energies. Consequently, the electron temperature is substantially higher than the bulk gas temperature [11]. This “non-thermal” mechanism allows for surface activation and oxidize copper without damaging the material under the surface [12].

Whereas many studies on both atmospheric pressure plasma jets and laser-induced plasmas have been published independently in the literature, there are very few studies comparing their basic spectroscopic and plasma diagnostic properties using controlled and comparable conditions. Previously, many researchers have concentrated on improving the efficiency of either one type of laser or one type of discharge source, but the way in which their respective excitation mechanisms of high-power photon-induced thermal ablation and low-energy gas-discharge collisional ionization influence the electron temperature and density dynamics of the plasma has not yet been fully understood. This study attempts to fill that void through a comparative spectroscopic study of copper plasma produced from an atmospheric plasma jet and a Neodymium-doped Yttrium Aluminum Garnet (Nd:YAG) laser.

II. Experimental Part

A. Plasma Jet Method

The plasma jet system is shown in Fig. 1. The experimental setup consists of a cold atmospheric plasma jet system, a copper electrode, argon (Ar) gas, a voltage regulator, and a high-voltage power supply. A 13 kV, 40 kHz power supply generates the plasma jet, which has open-circuit protection and works efficiently in typical atmospheric conditions. Argon gas flows into a needle cathode connected to the power supply. In order to collect plasma emissions, a quartz optical Fiber was positioned about 8 cm from the plasma plume and angled 45 degrees from the jet axis to enhance signal quality.

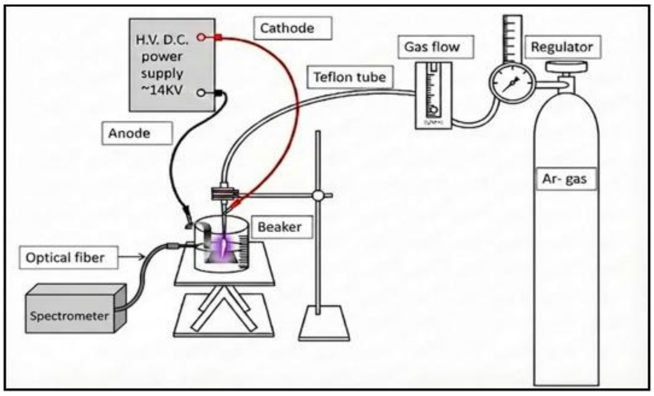

Fig. 1. Optical emission spectroscopy diagnostic and plasma jet system configuration.

B. Pulsed Laser Deposition Method

A pulsed laser was used to generate plasma from a solid Cu target. The setup of the laser-induced plasma spectroscopy (LIPS) experiment is described in Fig. 2. In this work, a Q-switched Nd:YAG pulsed laser (1064 nm wavelength, 6 Hz frequency, and 9.0 ns pulse duration) was utilized. The laser beam was aimed at the target at 45°. A plasma plume appears over the target's surface as the laser beam rapidly ionizes and evaporates the localized material. For both methods, the spectrum type is an S3000-UV-NIR Spectrometer.

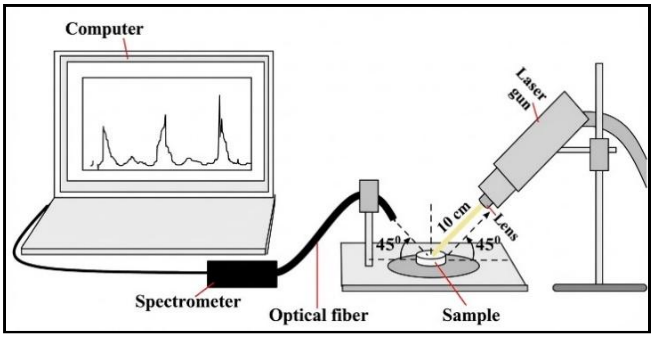

Fig. 2. Schematic illustration of the experimental LIBS setup.

C. Calculations of Plasma Parameters

After conducting experimental spectroscopic assessments of copper plasma produced through the Plasma Jet and Nd:YAG laser techniques, a quantitative analysis of the plasma characteristics was carried out. The collected emission spectra were scrutinized to obtain the essential plasma parameters that govern excitation and ionization processes. To accomplish this, standard spectroscopic formulas were utilized, operating under the premise of local thermodynamic equilibrium (LTE). The subsequent equations were employed to calculate electron temperature, electron density, and other derived plasma parameters required for the comparative evaluation.

1) Electron Temperature Calculation

To find the temperature of the electrons, the Boltzmann Plot method was utilized in the laboratory experiment based on the hypothesis that the plasma maintains local thermodynamic equilibrium [13]:

$$\ln\left[\frac{\lambda_{ji} I_{ji}}{hcA_{ji} g_j}\right] = -\frac{1}{kT}(E_j) + \ln\left|\frac{N}{U(T)}\right|, \qquad (1)$$

where I_{ji} is the relative intensity of the emission line between the energy levels i and j, λ_{ji} its wavelength, g_{ji} is the degeneracy or statistical weight of the emitting upper level i of the studied transition, and A_{ji} is the transition probability for spontaneous radiative emission from level i to the lower level j, E_j is the excitation energy of level i, k is the Boltzmann constant, and N state population density.

2) Electron Density Calculation

Electron density can be calculated using this equation [14].

$$n_e(\text{cm}^{-3}) = \left(\frac{\Delta\lambda}{2w_s}\right) N_r, \qquad (2)$$

where ω_s is the Stark broadening parameter contained in the standard tables corresponding to the Ar in plasma jet method and Cu in LIBS method. emission line at 309 nm wavelength; Nr is the reference electron density and is equal to (1 x 10^{17}) cm^{-3}.

3) Derived Plasma Parameters

Using the computed electron temperature and density, further plasma parameters were assessed. The plasma frequency (f_p) was determined with the following equation [15]:

$$f_p(Hz) = 8.98\sqrt{n_e} \qquad (3)$$

The Debye length (λ_D) was calculated by applying [16]:

$$\lambda_D(cm) = 743\sqrt{\frac{T_e}{n_e}} \qquad (4)$$

The Debye number (N_D) was derived using [17]:

$$N_D = \frac{4\pi}{3} n_e \lambda_D^3 \qquad (5)$$

4) Statistical Analysis

Statistical analysis was conducted utilizing SPSS software. The average (M) and standard deviation (SD) for all plasma parameters were directly extracted from the SPSS output. Given that the sample sizes for both groups were identical ($n_1 = n_2$), the pooled standard deviation S_p was determined using the simplified formula [18]:

$$S_P = \sqrt{\frac{S_1^2 + S_2^2}{2}}, \qquad (6)$$

where S_1 and S_2 signify the standard deviations of the plasma jet and Nd: YAG laser groups, respectively. The standardized mean difference (Cohen's d) was then calculated as follows [18]:

$$d = \frac{M_2 - M_1}{S_p}, \qquad (7)$$

where M_1 and M_2 represent the mean values of the two methods.

III. Results and Discussion

A. Comparison of OES Intensity for Plasma Jet and Nd:YAG Laser

Spectral examination of the copper plasma generated by both the Atmospheric Plasma Jet and Nd:YAG laser methods showed that the primary emission lines are associated with neutral copper (Cu I), with a minimal presence of ionic copper (Cu II) lines, especially in the ultraviolet spectrum, as illustrated in Figs. 3–5.

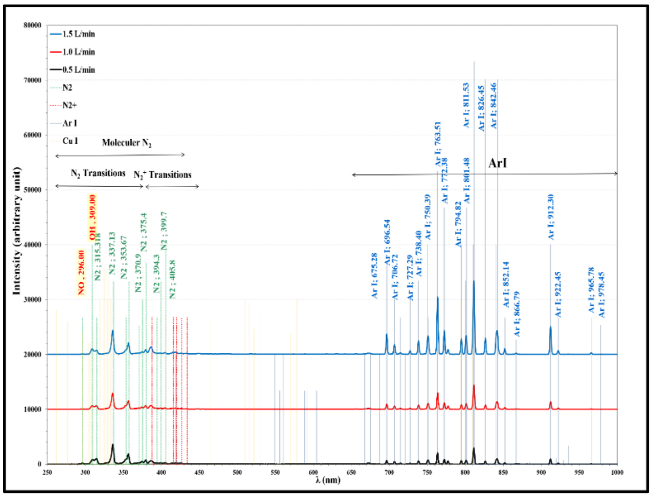

Fig. 3. OES of copper plasma generated by the plasma jet at different argon flow rates, showing Ar I and molecular nitrogen (N_2/N_2^+) emission lines.

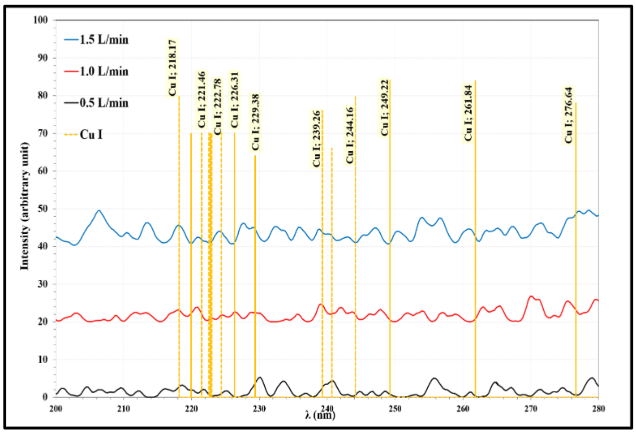

Fig. 4. The copper plasma jet emission spectra at various argon gas flow rates.

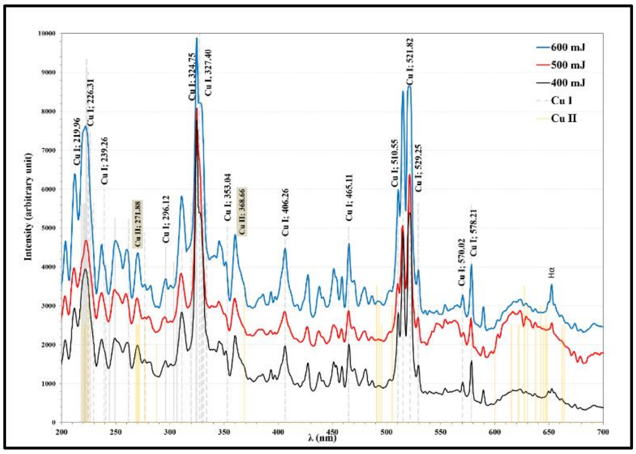

Fig. 5. The Laser Pulse emission spectra of copper at various energies.

For the plasma jet technique, emission spectra at various argon flow rates, i.e., 0.5 to 1.5 L/min, indicated that the overall emission intensity is higher at higher flow rates. This result is in line with what has been reported in [19]. This increase in intensity can be explained by better excitation efficiency and the high concentration of electrons at higher flow rates, which results in more frequent collisions between electrons and atoms, which in turn leads to stronger radiative transitions [20]. Moreover, there were clearly visible molecular nitrogen bands (N_2 and N_2^+) and Ar I lines that indicate how the gas is interacting with the air around it.

On the other hand, the plasma created by the Nd:YAG laser had much higher peak intensities for the Cu I transitions. his was especially evident at higher laser energies, such as 600 mJ. The increase in emission intensity as laser energy is increased is closely related to the higher photon energy density delivered onto the target surface [21]. This in turn leads to an increase in ablation efficiency, plasma temperature, and excitation possibility [22]. When compared under similar conditions, the plasma produced by the laser generally produced emission peaks that were stronger and more concentrated. The plasma jet, on the other hand, had different spectral profiles, with molecular and atomic particles. This is why plasma is formed in the laser and not the plasma jet, since laser ablation is photothermal and the plasma jet is electrical discharge excitation .These results suggest that the Nd:YAG laser is more effective in producing powerful emission of copper atoms. This makes it more suitable for applications that require strong excitation and very precise material removal, which is consistent with previous findings [23]. Conversely, the plasma jet system provides more consistent and steady excitation conditions, which are suitable for surface modification and coatings, and this is in line with reference [24].

B. Comparison of Electron Temperature Between Plasma Jet and Nd:YAG Laser Methods

The electron temperature for the atmospheric plasma jet and copper plasma produced by the Nd:YAG laser was evaluated using the Boltzmann plot based on equation (1). For the plasma jet system, we used some transitions of neutral argon (Ar I), whose spectroscopic parameters are available in Table I. Neutral copper (Cu I) lines were used for the laser plasma; all atomic information for them is given in Table II. Ar I lines were selected for the plasma jet due to the abundance of the working gas present in the discharge zone, while for the laser plasma, it is the Cu I lines were selected because their emission is due to the ablation of the copper.

TABLE I. MEASURED PARAMETERS OF SELECTED AR I LINES USED FOR THE BOLTZMANN PLOT AT DIFFERENT ARGON FLOW RATES

λ (nm)	$A_{ji} \cdot g_j$	E_i (eV)	E_j (eV)	(0.5 L /min)	(1.0 L /min) *Intensity*	(1.5 L /min)
696.5	1.92E +07	11.548	13.328	1748.7 96	3082.8 00	10398. 080
706.7	1.90E +07	11.548	13.302	196.30 4	323.16 0	1080.9 00
763.7	1.22E +08	11.548	13.172	1448.4 96	2093.5 60	7182.3 50
801.4	4.64E +07	11.548	13.095	632.39 2	1007.9 00	3362.9 00
811.5	2.32E +08	11.548	13.076	3020.5 50	5222.0 40	15993. 240

The spectroscopic parameters from Table I and Table II were used to build the Boltzmann plots, according to Eq. (1). Next, the logarithmic intensity was set against the upper energy (Ej). The electron temperature is then calculated from the slope of the straight-line regression. Fig. 6 and Fig. 7 show the resulting diagrams. They cover the plasma jet with different argon flow rates and the Nd:YAG laser plasma with various pulse energies.

TABLE II. FUNCTIONAL TEST SUMMARY

λ (nm)	$A_{ji}\cdot g_j$	E_i (eV)	E_j (eV)	(400 mJ)	(500 mJ) Intensity	(600 mJ)
406.76	1.26E+08	3.8167	6.8676	1991.15	1900.69	2473.94
465.41	3.04E+08	5.0721	7.7370	2015.73	1925.27	2621.44
511.06	8.00E+06	1.3889	3.8167	2777.78	2638.15	4194.69
515.63	2.40E+08	3.7859	6.1912	4916.42	4162.24	6480.83
522.30	4.50E+08	3.8167	6.1920	5506.39	5391.35	6505.41
530.03	8.72E+07	5.3951	7.7370	1401.18	1777.78	1883.97
570.76	9.60E+05	1.6422	3.8167	1283.28	1310.72	1118.58
578.84	3.30E+06	1.6422	3.7859	1647.00	1728.61	2203.54

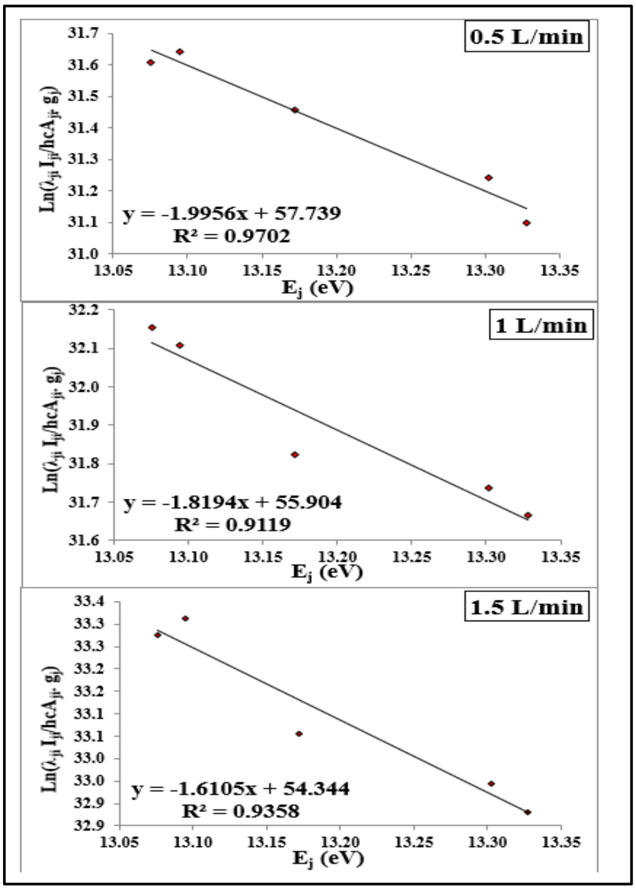

Fig. 6. The Laser Pulse emission spectra of copper at various energies.

In the plasma jet technique, there is a straight line connecting the logarithmic intensity value to the higher energy level, and this is true for all argon flow rates from 0.5 up to 1.5 L/min. Hence, we can see local thermodynamic equilibrium (LTE). In the laser-induced plasma with pulse energies between 400 and 600 mJ, the slope decreases as the flow rate for the plasma jet or the pulse energy of the laser is increased, which implies the electron temperature is also increased. The R^2 values were linear in all cases, so the spectroscopic study is reliable.

In a comparison of results, the plasma produced by the Nd:YAG laser has been found to have significantly higher electron temperature readings than the plasma jet under the test conditions, as shown in Table III. This is due to the very fast and focused laser energy transfer towards the copper target, leading to large material removal and high electron kinetic energy and better excitation efficiency [25]. In contrast, the plasma jet system distributes the energy across the discharge gas, which in turn moves slowly through collisions between electrons and atoms [26], and thus has a somewhat lower electron temperature. Hence, even though both systems meet the linearity requirement in Equation (1), the laser process has a hotter, more energetic plasma and the plasma jet has a more moderate level of gas-controlled excitation.

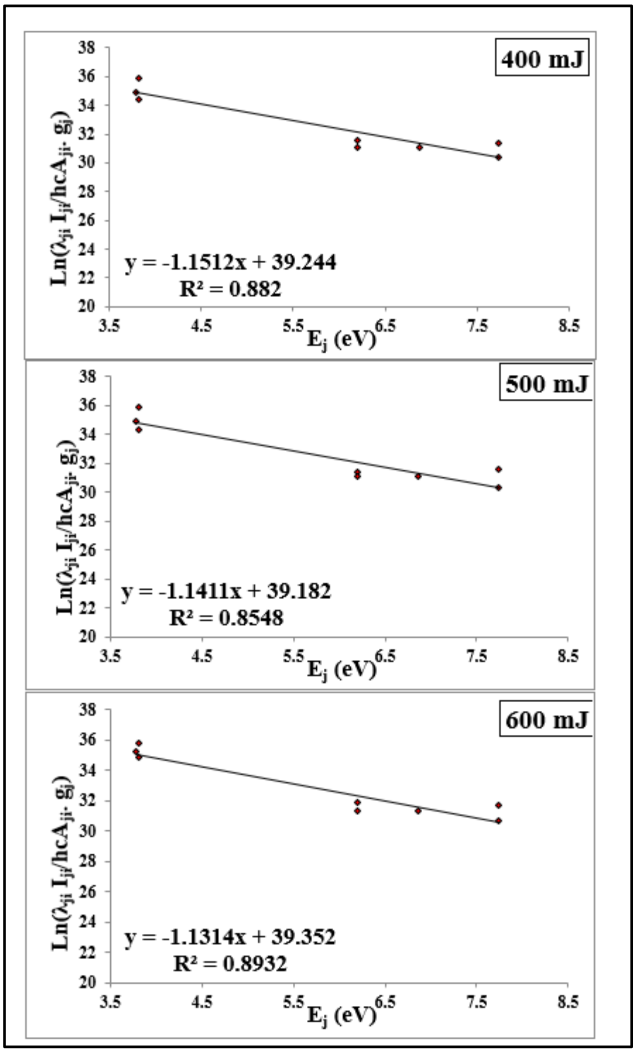

Fig. 7. Boltzmann plots of Cu I emission lines for electron temperature determination at different energies.

C. Comparison of Electron density Between Plasma Jet and Nd:YAG Laser Methods

The electron density measurements shown in Fig. 8 and Fig. 9 were done using Stark broadening of some selected emission lines. Lorentzian fitting was used here. In the case of the plasma jet setup, they picked the Ar I line at 763.5 nm. It was chosen because of its isolation from the plasma and a nice, symmetrical Lorentzian shape. However, with laser-induced plasma, the Cu I line is between 324 and 325 nm. This is important because it shows the direct emission from copper ablation.

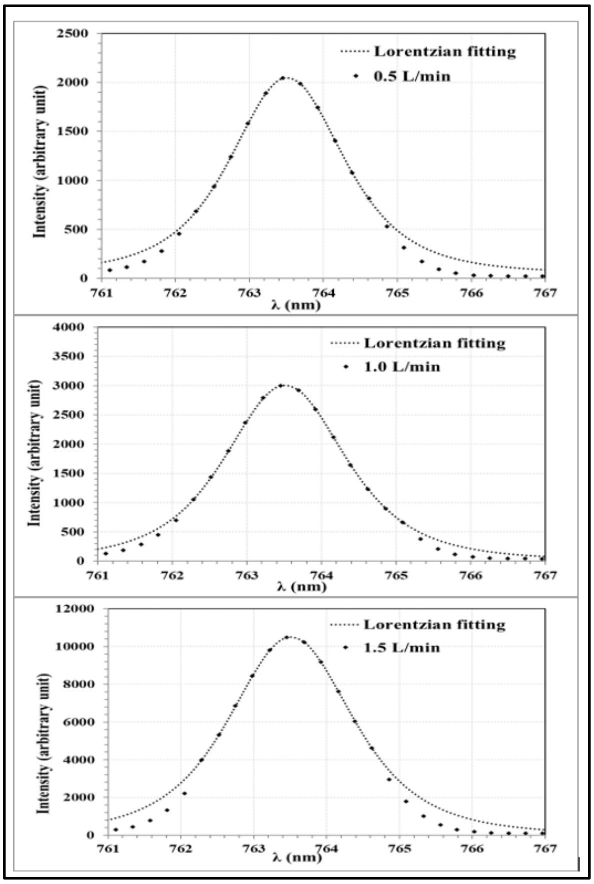

Fig. 8. Lorentzian fitting of the Ar I emission jet at different argon flow rates.

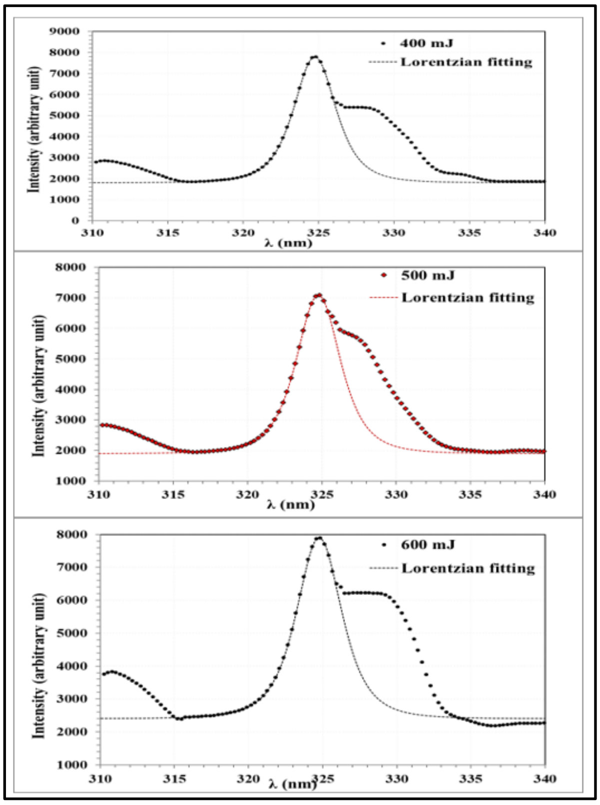

Fig. 9. Lorentzian fitting of the Cu I emission at different pulse energies.

According to Lorentzian curve fits, the full width at half maximum (FWHM) grows larger as the operational conditions become more intense in both systems. This is consistent with the results of [27] and [28]. However, the profiles created by the laser plasma are much broader than those from the plasma jet. Hence, in the same vein, the laser-generated plasma has more Stark broadening and hence a higher density of electrons.

The differences in these variations are probably due to the various processes involved in how plasma is formed. A laser pulse delivers high energy over a short duration within a highly confined area. This causes rapid ionization, resulting in an intense plasma plume. Such conditions promote strong Coulomb interactions between the charged particles, which in turn boosts the Stark broadening [29]. On the other hand, a plasma jet is propelled by a continuous discharge of electricity in the gas atmosphere. This method generally results in a lower instantaneous particle density and therefore a lower Stark broadening [30].

D. Comparison of plasma frequency, Debye length, and Debye number between Plasma Jet and Nd:YAG Laser Methods

Table III compares the plasma characteristics obtained in both experiments. The plasma frequency, which is directly affected by the electron density, is also identical for the values of fp. The plasma jet reached 1.044×10^{13} Hz, just a bit above what the laser actually recorded at 1.004×10^{13} Hz. However, this trend differs for the Debye length. The laser plasma is larger, from 6.25 to 6.47 $\times 10^{-6}$ cm, and is still far from the plasma jet, 4.77 to 5.04 $\times 10^{-6}$ cm. This rise in the Debye sphere's size is due to the increased electron temperature inside the laser system. The higher temperature increases the electrons' kinetic energy, which in turn decreases the electrostatic shielding performance. The Debye number is where the largest difference is made. The plasma created by the laser has ND values near 1300. This is almost twice as high as the plasma jet in 553 to 723. Therefore, the laser plasma operates deep within the collective and quasi-ideal plasma regime. In this case, Coulomb forces interacting over long distances are more important than a simple collision between two particles. The plasma jet is in a state of denser but cooler plasma, with more robust screening and plasma arrangement controlled by the discharge.

TABLE III. PLASMA PARAMETERS FOR TWO METHODS: PLASMA JET AND LASER

Method (Variable)	Te (eV)	FWHM (nm)	ne $\times 10^{18}$ (cm^{-3})	fp $\times 10^{13}$ (Hz)	λD $\times 10^{-6}$ (cm)	ND
Plasma Jet (0.5 L/min)	0.501	1.80	1.216	0.990	4.769	553
Plasma Jet (1.0 L/min)	0.550	1.90	1.284	1.018	4.862	618
Plasma Jet (1.5 L/min)	0.621	2.00	1.351	1.044	5.036	723
Nd:YAG Laser (400 mJ)	0.869	3.30	1.146	0.962	6.470	1299
Nd:YAG Laser (500 mJ)	0.876	3.50	1.216	0.990	6.310	1278
Nd:YAG Laser (600 mJ)	0.884	3.60	1.251	1.004	6.250	1277

The discrepancy between electron temperature and electron density in copper plasmas for both approaches stems from the excitation and energy-transfer mechanisms inherent to each method. For plasma-jet excitation, the excitation process depends on electron collisions and on quasi-steady collisions produced by the discharge of inert argon gas. As a result, an average temperature is obtained, and increasing the gas flow rate strengthens the collisions, which in turn causes electron density to rise gradually [30]. For pulsed-laser excitation, the excitation process is driven by intense heating of the copper target, thereby forming a plasma column with strong local dynamic confinement. This produces a high temperature, reaching as much as 0.88 electron volts [31].

E. Validation of Local Thermodynamic Equilibrium (LTE) in Plasma Jet and Nd:YAG Laser Methods

Using the McWhirter criterion [32]:

$$N_e \geq 1.6 \times 10^{12} T^{\frac{1}{2}} (\Delta E)^3, \quad (8)$$

the critical minimum electron densities were determined and were found to fall in the range of about 10^{12}-10^{13} cm^{-3}. As shown in Table III, the experimentally measured electron densities obtained from Stark broadening of the Ar I and Cu I spectral lines lie between (1.14×10^{18} and 1.35×10^{18} cm^{-3}). Because the actual electron densities are greater than the McWhirter threshold by several orders of magnitude, the LTE assumption is convincingly validated for both the plasma jet and the Nd:YAG laser-produced copper plasma in the operational conditions studied.

F. Statistical Analysis for Plasma Parameters

The statistical analysis of the plasma parameters obtained from the plasma jet and Nd:YAG laser methods is presented in Table IV and Fig. 10. The pooled standard deviation (Sp) and Cohen's d were used to evaluate the size and direction of the differences between the plasma jet and the Nd:YAG laser methods.

TABLE IV. PLASMA STATISTICAL ANALYSIS FOR TWO METHODS: PLASMA JET AND LASER

Plasma Parameter	Plasma Jet (Mean ± SD)	Nd:YAG Laser (Mean ± SD)	Sp	Cohen's d
Te (eV)	0.557 ± 0.060	0.876 ± 0.008	0.043	+7.420
FWHM (nm)	1.900 ± 0.100	3.467 ± 0.153	0.129	+12.135
ne $\times10^{18}$ (cm^{-3})	1.284 ± 0.068	1.204 ± 0.053	0.061	−1.303
fp $\times10^{13}$ (Hz)	1.017 ± 0.027	0.985 ± 0.021	0.024	−1.314
λD $\times10^{-6}$ (cm)	4.889 ± 0.136	6.343 ± 0.114	0.125	+11.625
ND	631.333 ± 85.781	1284.667 ± 12.423	61.289	+10.660

In the case of electron temperature, a large effect size (d = +7.420) was observed. This indicates that the plasma produced by the Nd:YAG laser is much hotter than the plasma jet. For the FWHM values (d = +12.135), an even larger impact was seen, which adds weight to the picture that the laser-generated plasma is more clearly Stark broadening. However, when looking at the electron density (ne), the effect size was actually negative (d= -1.303). This suggests that the plasma jet has slightly higher electron density than the laser setup. We also observed the same trend on plasma frequency (fp) where the d-value is negative (d = -1.314) which is quite consistent with how directly it relates to electron density. In contrast, we observed large positive effect sizes at both Debye length (d = +11.625) and Debye number (d = +10.660). These results indicate that the laser-produced plasma operates in a state dominated by thermal energy and collective interaction. This is reflected in its larger Debye spheres and the overall plasma dynamics. The plasma jet system, although a bit denser, tends to stay cooler and is more determined by its discharge properties.

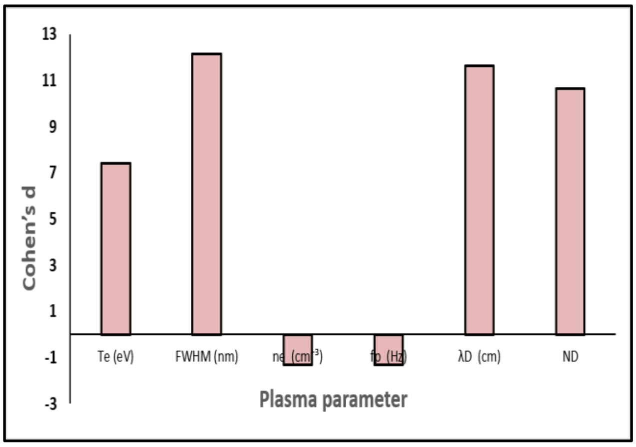

Fig. 10. Statistical Effect Size Analysis of Plasma Parameters for Plasma Jet and Nd:YAG Laser Techniques.

The uncertainty associated with the calculated plasma parameters mostly stems from the precision of spectral line measurements as well as the fitting process in the Boltzmann and Stark methods. The wavelength resolution of the spectrometer was ±0.02 nm, thus causing an uncertainty while measuring the spectral line position and width. Therefore, the uncertainty of the calculated electron temperature and electron density was ±5%.

IV. CONCLUSION

The plasma generated by the laser method has much more intense electron heating, a much broader spectral range, and better collective behavior of the plasma itself. It certainly suggests a regime where thermal dynamics are dominant, and energy levels are quite high. The plasma jet provides a discharge plasma setting that is much denser but at the same time cooler and is a lot more controlled. More importantly, the statistical review confirms these results. This statistically significant difference confirms that the variations between the two methods are inherent to their distinct plasma creation mechanisms. In the plasma jet, there is a continuous gas discharge, whereas in the laser system, there is a transient, high-energy ablation process.

REFERENCES

[1] M. A. Issa and K. A. Aadim, "Influence of ZnO nanoparticles prepared by plasma jet and laser ablation on fungi, gram positive and gram negative bacteria," *AIP Conference Proceedings*, vol. 3177, 2026, doi: 10.1063/5.0318094.

[2] J. Simons, "Theoretical study of negative molecular ions," Annual Review of Physical Chemistry, vol. 62, no. 1, pp. 107–128, 2011, doi: 10.1146/annurev-physchem-032210-103547.

[3] A. S. Zhakypov, R. R. Nemkayeva, Y. Yerlanuly, M. A. Tulegenova, B. Y. Kurbanov, M. B. Aitzhanov, *et al*., "Synthesis and in situ oxidation of copper micro- and nanoparticles by arc discharge plasma in liquid," *Scientific Reports*, vol. 13, no. 1, p. 15714, 2023, doi: 10.1038/s41598-023-41631-2.

[4] A. M. Ahmed, M. M. Halim, N. M. Ahmed, M. Rashid, and B. A. Taha, "Advances in pulsed laser ablation in liquid for silver and copper synthesis: From plasma generation to nanoparticle formation," *physica status solidi (a)*, vol. 222, no. 18, p. 2500382, 2025, doi: 10.1002/pssa.202500382.

[5] A. Rydosz, "The use of copper oxide thin films in gas-sensing applications," *Coatings*, vol. 8, no. 12, p. 425, 2018, doi: 10.3390/coatings8120425.

[6] M. Nolan, S. D. Elliott, J. S. Mulley, and K. P. McKenna, "Tuning the electronic structure of the transparent conducting oxide Cu2O," *Thin Solid Films*, vol. 516, no. 7, pp. 1468–1472, 2008, doi: 10.1016/j.tsf.2007.03.073.

[7] R. Katal, S. Masudy-Panah, E. Y.-J. Kong, N. Dasineh Khiavi, and others, "Nanocrystal-engineered thin CuO film photocatalyst for visible-light-driven photocatalytic degradation of organic pollutant in aqueous solution," *Catalysis Today*, vol. 340, pp. 236–244, 2020, doi: 10.1016/j.cattod.2018.12.019.

[8] M. A. Issa, "Influence of Ar Gas Flow Rate on the Properties and Coupling Behavior of Iron Plasma," *Iraqi Journal of Applied Physics*, vol. 22, no. 2, pp. 317–321, 2026, doi: 10.2025/1qkzen10.

[9] M. Issa and K. A. Aadim, "Influence of gas flow rate on the plasma temperature and electron density of an atmospheric argon plasma jet," *Jordan Journal of Physics*, vol. 18, no. 4, pp. 435–442, 2025, doi: 10.47011/18.4.

[10] Q. Su, C. Zuo, M. Liu, and X. Tai, "A review on Cu_2O-based composites in photocatalysis: Synthesis, modification, and applications," *Molecules*, vol. 28, no. 14, p. 5576, 2023, doi: 10.3390/molecules28145576.

[11] P. J. Bruggeman, F. Iza, and R. Brandenburg, "Foundations of atmospheric pressure non-equilibrium plasmas," *Plasma Sources Science and Technology*, vol. 26, no. 12, p. 123002, 2017, doi: 10.1088/1361-6595/aa97af.

[12] J. Zhou, T. Wei, and X. An, "Combining non-thermal plasma technology with photocatalysis: A critical review," Physical Chemistry Chemical Physics, vol. 25, no. 3, pp. 1538–1545, 2023, doi: 10.1039/d2cp04836a.

[13] J. Mrotzek and W. Viöl, "Spectroscopic characterization of an atmospheric pressure plasma jet used for cold plasma spraying," *Applied Sciences*, vol. 12, no. 13, p. 6814, 2022, doi: 10.3390/app12136814.

[14] M. A. Issa and K. A. Aadim, "Optical emission spectroscopy of zinc oxide doped nickel oxide to calculate plasma parameters using the Boltzmann plot method," *Iraqi Journal of Physics*, vol. 23, no. 2, pp. 118–127, 2025, doi: 10.30723/ijp.v23i2.1230.

[15] H. M. Abdulwahab and H. R. Humud, "Plasma characterization of microwave plasma jet at atmospheric pressure," *Iraqi Journal of Science*, pp. 151–159, 2024, doi: 10.24996/ijs.2024.65.1.14.

[16] A. A. Hussain, "Plasma characteristics of Ag:Al alloy produced by fundamental and second harmonic frequencies of Nd:YAG laser," *Iraqi Journal of Physics*, vol. 14, no. 31, pp. 205–214, 2016, doi: 10.30723/ijp.v14i31.188.

[17] D. K. Naser and M. J. Kadhim, "Diagnostics of tin and cadmium plasma produced by Nd:YAG (1064 nm) laser," in *AIP Conference Proceedings*, vol. 2839, no. 1, p. 080015, Sep. 2023, doi: 10.1063/5.0171218.

[18] D. A. Fitts, "Point and interval estimates for a standardized mean difference in paired-samples designs using a pooled standard deviation," The Quantitative Methods for Psychology, vol. 18, no. 2, pp. 207–223, 2022, doi: 10.20982/tqmp.18.2.p207.

[19] M. H. Ahmed and H. R. Humud, "Investigating the impact of gas type and gas flow rate on plasma jet parameters by optical emission spectroscopy," *Letters in High Energy Physics*, vol. 2714, pp. 3615–3629, 2024.

[20] C. S. Ponseca Jr., P. Chábera, J. Uhlig, P. Persson, and V. Sundström, "Ultrafast electron dynamics in solar energy conversion," *Chemical Reviews,* vol. 117, no. 16, pp. 10940–11024, 2017, doi: 10.1021/acs.chemrev.6b00807.

[21] M. Fikry, W. Tawfik, and M. M. Omar, "Investigation on the effects of laser parameters on the plasma profile of copper using picosecond laser induced plasma spectroscopy," *Optical and Quantum Electronics,* vol. 52, no. 5, p. 249, 2020, doi: 10.1007/s11082-020-02381-x.

[22] A. De Giacomo, R. Alrifai, V. Gardette, Z. Salajková, and M. Dell'Aglio, "Nanoparticle enhanced laser ablation and consequent effects on laser induced plasma optical emission," *Spectrochimica Acta Part B: Atomic Spectroscopy*, vol. 166, p. 105794, 2020, doi: 10.1016/j.sab.2020.105794.

[23] A. Taylan, "Synthesis of nanoparticles by laser ablation in liquid method and optical applications," *M.S. thesis*, Bilkent University, Ankara, Türkiye, 2023.

[24] K. G. Kostov, T. M. C. Nishime, A. H. R. Castro, A. Toth, and L. R. D. O. Hein, "Surface modification of polymeric materials by cold atmospheric plasma jet," *Applied Surface Science*, vol. 314, pp. 367–375, 2014, doi: 10.1016/j.apsusc.2014.07.009.

[25] J. Wu, Y. Zhou, M. Chen, and X. Li, "Numerical modeling and simulation on nanosecond laser-target interactions," *Journal of Physics D: Applied Physics*, vol. 58, no. 14, p. 143004, 2025, doi: 10.1088/1361-6463/adb58f.

[26] X. Li et al., "Plasma bullet splitting behavior of a positive streamer initiated in an atmospheric pressure argon plasma jet," *Physics of Plasmas*, vol. 32, no. 5, 2025, doi: 10.1063/5.0250358.

[27] S. N. AlRashid, N. F. Majeed, M. A. Azeez, and S. N. Mazhir, "Calculating plasma parameters for Zn target using laser-induced breakdown spectroscopy," *Journal of Optics*, pp. 1–7, 2025, doi: 10.1007/s12596-025-02644-4.

[28] Y. A. Ali and R. A. Khamis, "Spectroscopic study of copper plasma produced by Nd:YAG laser from the nano and bulk copper targets," in Journal of Physics: Conference Series, vol. 1818, no. 1, p. 012008, Mar. 2021, doi: 10.1088/1742-6596/1818/1/012008.

[29] M. Bailly-Grandvaux, "Laser-driven strong magnetic fields and high discharge currents: Measurements and applications to charged particle transport," Ph.D. dissertation, Université de Bordeaux, 2017.

[30] P. Viegas et al., "Physics of plasma jets and interaction with surfaces: Review on modelling and experiments," Plasma Sources Science and Technology, vol. 31, no. 5, p. 053001, 2022, doi: 10.1088/1361-6595/ac61a9.

[31] G. Mehdi et al., "Low-Temperature Plasma-assisted Ammonia Combustion to enhance Ignition, Flame Speed, and NOx Characteristics," Applications in Energy and Combustion Science, p. 100539, 2026, doi: 10.1016/j.jaecs.2026.100539.

[32] S. Shilpa et al., "Colliding laser-produced plasmas: progress and perspectives," Journal of Physics D: Applied Physics, vol. 59, no. 26, p. 263002, 2026, doi : 10.1088/1361-6463/ae7a7f.

[33] P. Chu et al., "One-point calibration of underwater double-pulse laser-induced breakdown spectroscopy," Spectrochimica Acta Part B: Atomic Spectroscopy, vol. 237, p. 107455, 2026, doi: 10.1016/j.sab.2026.10745.